Anal Bioanal Chem (2015) 407:8225–8231
DOI 10.1007/s00216-015-8974-x

RESEARCH PAPER

Plasmonic vertical dimer arrays as elements for biosensing

Andreas Horrer[1] · Katrin Krieg[2] · Kathrin Freudenberger[2] · Sabrina Rau[2] · Lothar Leidner[2] · Günter Gauglitz[2] · Dieter P. Kern[1] · Monika Fleischer[1]

Received: 16 April 2015 / Revised: 5 August 2015 / Accepted: 12 August 2015 / Published online: 7 September 2015

Abstract Localized surface plasmon resonances of metallic nanoparticles can be used for biosensing because of their sensitive dependence on the refractive index of the surrounding medium. The binding of molecules to the particles causes a change of the effective refractive index in their close vicinity, which leads to a reversible shift of the resonance. We present simulations and sensing experiments of a plasmon resonance based biosensor that makes use of the narrow antisymmetric resonance in coupled plasmonic vertical dimers. The sensitivity of the antisymmetric resonance is compared with that of a surface lattice resonance for refractive index sensing of bulk and of thin layers of molecules. The functionality of such a sensor surface is demonstrated via a testosterone immunoassay for detection of antibody from a solution by binding to surface-immobilized antigen in a fluidic channel.

Keywords Plasmonic nanostructures · Biosensing · Label-free immunoassay · Vertical dimer · Testosterone

Published in the topical collection *Nanospectroscopy* with guest editor Mustafa Culha.

✉ Andreas Horrer
andreas.horrer@uni-tuebingen.de

✉ Monika Fleischer
monika.fleischer@uni-tuebingen.de

[1] Institute for Applied Physics and Center LISA+, University of Tübingen, Auf der Morgenstelle 10, 72076 Tübingen, Germany

[2] Institute of Physical and Theoretical Chemistry, University of Tübingen, Auf der Morgenstelle 18, 72076 Tübingen, Germany

Introduction

Lab-on-a-chip detection is becoming increasingly important for point-of-care applications, including the detection of viruses, and hand-held applications, e.g. water monitoring. Therefore small, label-free sensors with fast read-out are required. One possibility is to make use of plasmonic nanostructures. When excited by light, metallic nanoparticles have a resonance in their spectrum, which is referred to as a localized surface plasmon resonance (LSPR). The resonance wavelength depends, among other parameters, on the refractive index of the particles' surrounding. The approach of using this dependency for sensing applications, e.g. for the detection of biomolecules [1–6] or as gas sensors [7], has been pursued for some time. Different kinds of particle, including nanopyramids [8], colloidal nanoparticles [9], nanorods [10], nano-islands [11], elliptical nanodiscs [12], and nanotriangles [13], have been investigated, using either single or ensembles of particles.

An advantage of LSPR sensors over other established sensing methods, for example chemiluminescence [14] or fluorescence-based immunoassays [15], is that the analyte does not have to be labeled, because its very presence after binding to the recognition structure modifies the detection signal. The time scale for such an immunoassay is very short, typically only a few minutes, and even real-time binding kinetics can be studied. Furthermore, the detection volume can be chosen to be very small. The small area for optical read-out, of a few micrometers squared or even less, combined with the implementation in a microfluidic channel, enables application as lab-on-a-chip.

The specific binding of an analyte to a recognition structure at the surface of a nanoparticle causes a small change in the effective refractive index of the particle's surrounding. This leads to a shift of the resonance in the optical extinction spectrum of the particle. Even single binding events may be detectable by this technique [16].

The sensitivity of sensors based on LSPR shifts can be characterized by the shift of the resonance per refractive index unit (RIU). The figure of merit (FOM) is defined as the ratio of the sensitivity to the resonance linewidth [17].

The FOM may be used as a measure of the quality of the sensor. The higher the FOM, the better even small changes of the refractive index should be detectable. Typical sensitivities of the resonance of plasmonic nanostructures are of the order of several hundred nanometers per refractive index unit. For typical linewidths of plasmonic resonances of several tens of nanometers, this results in standard FOMs well below 10. High FOMs could, e.g., be achieved for very narrow Fano resonances. This has been revealed for plasmonic nanohole arrays, which yielded FOMs of over 100 [18].

Strong shifts and a small resonance linewidth are beneficial for the detection of even small concentrations of biomolecules, which result in a low coverage of the particles' surface with molecules. Periodically arranged nanostructures can additionally have narrow features in their extinction spectra caused by interaction of the nanostructures with the light diffracted by the array [19, 20]. This resonance arises at the wavelength matching the lattice constant of the array multiplied with the refractive index of the surrounding. It is referred to as the surface lattice resonance (SLR). The SLR is most pronounced and narrow in an index-matched environment [21]. Biomolecular detection mostly takes place in a water environment (n=1.33). For that reason the index of the substrate in this work has been adjusted by using a magnesium fluoride layer (n=1.38) instead of glass (n=1.51).

This work concentrates on arrays of plasmonic vertical dimers. They consist of two metal discs stacked as a sandwich with a narrow dielectric spacer in between (Fig. 1a). They typically have two resonances in their spectra when excited with light polarized perpendicular to the dimer axis [22, 23]. These resonances originate from plasmon hybridization resulting from coupling of the discs [24]. The first mode is a symmetric mode with the dipole moments in the nanodiscs oriented parallel to each other, which occurs at wavelengths near the resonance of a single disc. A second, antisymmetric mode with antiparallel dipole moments appears at lower energies. This mode is also referred to as a magnetic dipole mode, because the magnetic field in the spacer between the discs has a dipolar appearance [25]. Vertical dimers may also be used for surface-enhanced Raman scattering, because their two resonances can simultaneously enhance the excitation and the scattered wavelengths [26]. This geometry is chosen because, as simulations indicate, the linewidth of the antisymmetric resonance is smaller than that of the symmetric resonance or the resonance of single discs. As far as we are aware, regular arrays of vertical dimers have not been applied to molecular sensing before. Figure 1b shows the simulated transmission of light through samples with a single disc with a resonance at 620 nm, a vertical dimer with two resonances at 590 nm and 845 nm, and a periodic arrangement of vertical dimers in a square array with an additional SLR. The refractive index sensitivities of the antisymmetric dimer resonance and the SLR are investigated by simulations and optical measurements, and by molecular sensing in a fluidic channel.

Materials and methods

Simulations

The spectrally resolved extinction and the distribution of the electrical near-field of periodic arrays of vertical dimers were simulated using the finite element method with COMSOL Multiphysics. The model was built as a cuboid with an in and out port for electromagnetic excitation, with the electric field of intensity I_0 polarized parallel to the substrate on the top and on the bottom, respectively. Periodic boundary conditions were applied to the surfaces on the sides. The extinction was evaluated at the out port. From the transmitted intensity I_T, extinction spectra are calculated using $(I_0-I_T)/I_0$. In the

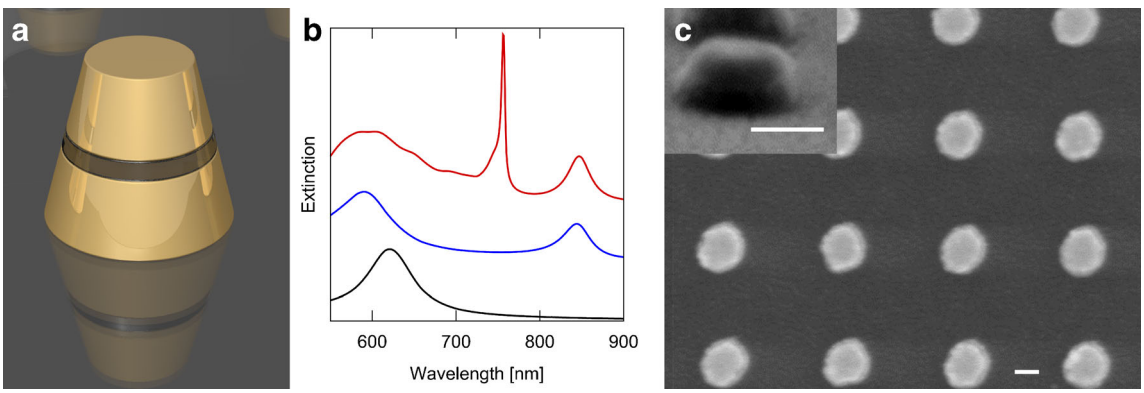

Fig. 1 (**a**) Schematic of the vertical gold–SiO_2–gold dimers. (**b**) Comparison of the simulated extinction spectra of a single disc with one resonance at 620 nm (*black, bottom*), a vertical dimer with a symmetric and an antisymmetric resonance at 590 nm and 845 nm, respectively (*blue, middle*), and an array of vertical dimers with an additional SLR at 755 nm (*red, top*). The curves are offset for clarity. (**c**) SEM image of an array of vertical dimers in top-view and of a single structure under a viewing angle of 75 °. The size of the scale bars is 100 nm

extinction spectrum, plasmon resonances appear as peaks. For the refractive index and the absorption coefficient of gold the data from Johnson and Christy were used [27]. The refractive index of the cuboid was set to 1.38 in the lower half (magnesium fluoride substrate) and to 1.33 in the upper half (water immersion). For the spectrally resolved evaluation of the overall near-field the normalized electric field strength was integrated over the particle's surface. In the near-field spectra the resonances are visible as peaks. To evaluate the spatially resolved distribution of the near-field, the normalized electric field strength E/E_0 was evaluated in every point of a cross-sectional plane through the particle normal to the substrate surface and along one of the array axes.

Fabrication

The vertical dimers were fabricated on 18 mm × 18 mm microscope glass coverslips (thickness approximately 130 μm), which had been previously covered with a layer of 500 nm magnesium fluoride (n=1.38) by thermal evaporation. A double layer of PMMA (total thickness approximately 300 nm) was spin coated onto the samples, followed by the deposition of a 15 nm layer of aluminium by thermal evaporation to ensure conductivity during electron-beam lithography. The resist was exposed with a Philips XL30 scanning electron microscope, with an energy of 30 keV and doses from 30 fC to 150 fC, to form patterns of circles of different diameters and distances after chemical development in a mixture of isopropanol and methyl isobutyl ketone. This was followed by the deposition of a sandwich of gold and silicon dioxide layers with the desired thicknesses by thermal and electron-beam evaporation, respectively. During the evaporation the diameter of the holes in the resist decreases laterally as a result of deposition on top of the resist, which leads to slightly tapered structures. A lift-off yielded the arrays of vertical dimer structures. Figure 1c shows an array of vertical dimers in top-view and a single vertical dimer under an angle of 75°.

For the fabrication of a microfluidic channel a mold was created by structuring SU-8 resist by optical lithography on a silicon wafer. PDMS (Sylgard 184) was poured onto the mold, hardened at 150 °C on a hotplate for 15 min, and peeled off. Holes were punched into the PDMS sheet to enable the connection of tubes. A glass coverslip with nanostructures was brought into contact with the PDMS to form a closed channel. The adhesion was promoted by activating the PDMS surface in an oxygen plasma. The channel had a length of 1.5 cm and a width of 200 μm. The channel height was 100 μm.

Optical characterization

The samples were characterized by optical extinction measurements in an inverted microscope (Nikon Eclipse Ti-U). The PDMS flow cell with the glass sample was illuminated by collimated white light incident perpendicular to the sample surface. A halogen lamp with a linear polarizer was used. The transmitted light was collected by an objective (20×, NA= 0.5). By use of a pinhole, only light originating from a circle with a diameter of 10 μm in the object plane was selected and guided to a spectrometer (Ocean Optics QE 6500) to measure the transmission spectra. The extinction was derived from the transmission as described in the "Simulations" section.

Reagents and materials

6-Amino-1-hexanethiol hydrochloride, dimethylformamid, *N*, *N*′-diisopropylcarbodiimide, sodium dodecyl sulfate (SDS), testosterone 3-(*O*-carboxymethyl)oxime, and all common chemicals were purchased from Sigma–Aldrich, Deisenhof, Germany. Monoclonal mouse antibodies to testosterone (IgG1, Clone 7003) and polyclonal antibodies to mouse IgG were purchased from Acris Antibodies GmbH, Herford, Germany. For regeneration of the sensor surface, a solution of 0.5 % SDS (*w*/*v*, pH 1.5) in Milli-Q water was used. As buffer solution phosphate-buffered saline (PBS) was prepared using 150 mmol L^{-1} NaCl and 10 mmol L^{-1} KH_2PO_4, and the pH was adjusted to 7.4.

Results and discussion

Characterization of vertical dimer arrays

To characterize the vertical dimers, simulations of the near-field of two gold discs with heights of 40 nm, separated by a dielectric (n=1.46) spacer, were performed. The disc diameter and the spacer thickness were varied. As a result of the fabrication process, the experimental dimers are slightly tapered. This fact was taken into account in the simulations with an angle of the sidewalls of 17 ° as measured by SEM. The polarization of the exciting electromagnetic field was parallel to the plane of the substrate. In Fig. 2a the spacer thickness was kept constant at 10 nm, and the base diameter was varied from 60 nm to 130 nm in 10 nm steps. The antisymmetric mode, which overlaps with the symmetric mode for small disc dimensions, shifts to larger wavelengths when the diameter is increased. A similar behavior is observed when decreasing the spacer thickness while keeping the diameter constant. In Fig. 2b the base diameter was kept constant at 100 nm, and the spacer thickness was varied from 25 nm to 5 nm, which shifts the antisymmetric resonance from overlapping with the symmetric mode to a wavelength of approximately 900 nm. The curves were vertically offset in both cases for clarity. As can be seen in the simulations, the linewidth of the antisymmetric mode is smaller than that of the symmetric mode. This makes it better suited for refractive index sensing. It can be shifted over a large wavelength range by varying the diameter of the discs and/or the spacer thickness. The near-

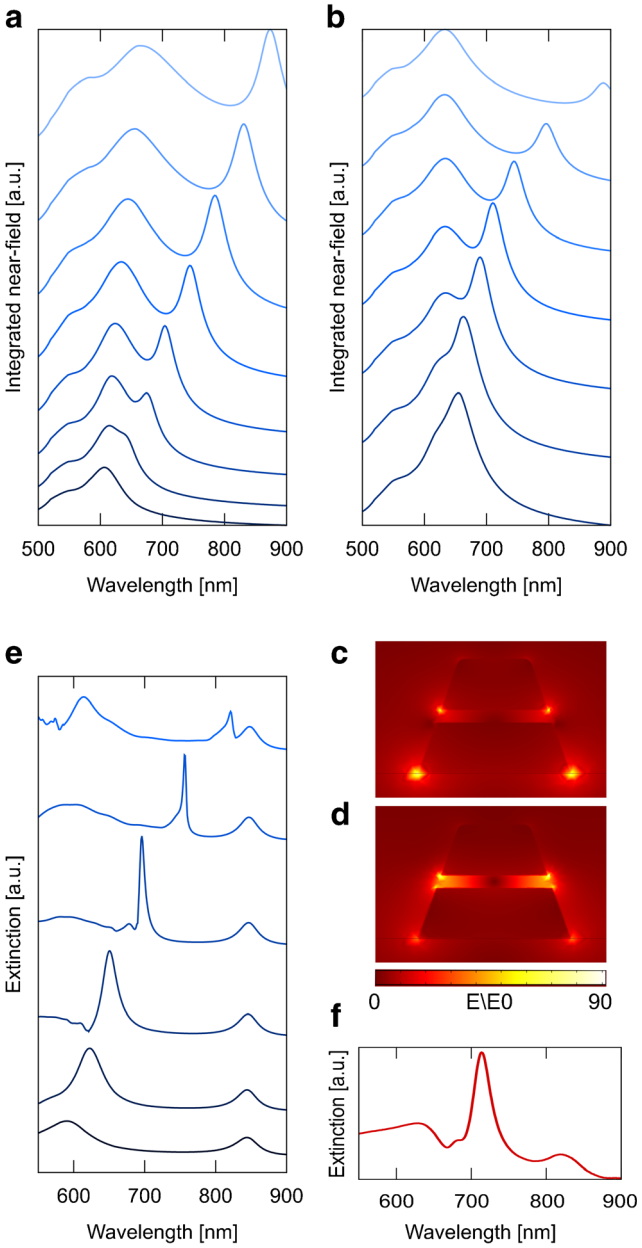

Fig. 2 (**a**, **b**) Simulations of the normalized near-field strength integrated over the surface of vertical dimers. In (**a**) the base diameter is varied from 60 nm to 130 nm (*bottom to top*) in 10 nm steps with a fixed spacer of 10 nm. In (**b**) the spacer thickness is 25 nm, 20 nm, 15 nm, and down to 5 nm in 2.5 nm steps (*bottom to top*) with a fixed base diameter of 100 nm. Increasing the diameter or decreasing the spacer thickness leads to a redshift of the antisymmetric resonance. (**c**, **d**) The near-field distributions of (**c**) the symmetric mode and (**d**) the antisymmetric mode in units of E/E_0. (**e**) Simulated extinction spectra for random distribution (*bottom*) and arrays with periods varying from 400 nm to 600 nm (*second from bottom to top*) in 50 nm steps. (**f**) Experimental extinction spectrum of vertical dimers with a diameter of 120 nm, a disc height of 40 nm, a 10 nm silicon dioxide spacer, and a period of 505 nm. The curves in (**a**), (**b**), and (**e**) are offset for clarity

field maps (Fig. 2c, d) show that the distribution of the electric field strength for the symmetric mode is similar to the case of single discs with hotspots at the edges, and particularly at the bottom edge. For the antisymmetric mode the electric field is mainly located between the discs in the dielectric spacer and just outside the spacer. This means the spots of high field intensity are shifted away from the substrate further into the surrounding medium, which could be beneficial for molecular sensing.

Figure 2e shows simulated extinction spectra of a non-periodic arrangement of vertical dimers (bottom) and of arrays with varying periods of 400 nm to 600 nm in 50 nm steps. The antisymmetric mode occurs at approximately 850 nm, and the SLR is shifted through the spectrum for different particle distances. Figure 2f shows an extinction measurement of a vertical disc array with a period of 505 nm. The symmetric dimer resonance occurs at approximately 635 nm, the antisymmetric resonance at approximately 820 nm. The position of the SLR at 715 nm is in accordance with the simulations. Compared with the simulations the SLR in the optical measurements is broader, which could be caused by lattice inhomogeneity.

Sensitivity tests

The sensitivity of the periodic arrays of vertical dimers to changes in the refractive index was examined by immersing a sample in solutions of water (n=1.33) and glycerin (n=1.47) with different mixing ratios in a flow cell. The solutions were prepared such that their refractive index changes in steps of 0.01. Figure 3a shows extinction spectra of vertical dimers in

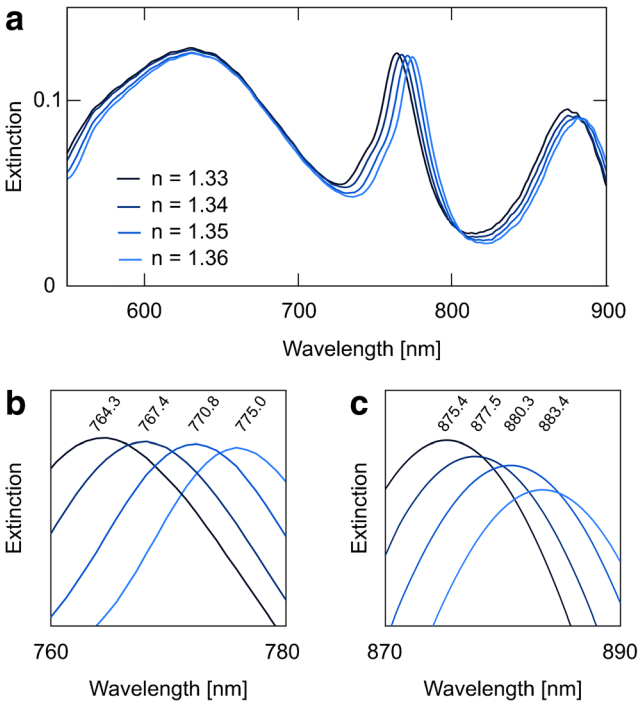

Fig. 3 (**a**) Sensitivity measurements in water–glycerin solutions with different mixing ratios to vary the refractive index. The zooms into (**b**) the SLR and (**c**) the antisymmetric resonance show the shifting peak wavelengths in the solutions with refractive indices from 1.33 to 1.36 in steps of 0.01 (*left to right*)

solutions with n=1.33–1.36. As can be seen in the zooms on the SLR and the antisymmetric mode in Fig. 3b, c, the position of the resonance wavelength depending on the refractive index progresses nearly linearly, and the shift in the different solutions gives sensitivities for the SLR and the antisymmetric dimer resonance of 326 nm and 248 nm per RIU, respectively. The line-width of the SLR is 38 nm, resulting in a FOM of ca. 8.6. The linewidth of the antisymmetric dimer resonance is 62 nm, giving a reasonable FOM of 4. The sensitivity of the symmetric resonance, which occurs at approximately 630 nm, of 110 nm per RIU is comparatively low.

Figure 4a shows the results of simulations of the refractive index sensitivity. Two cases were considered either by changing the bulk dielectric, or by changing the refractive index of only a 7 nm thin layer around the structure to simulate biomolecule adsorption. For the bulk simulations the refractive index was changed from 1.33 to 1.35. For the molecules an index of 1.5 was assumed. As can be seen in the zooms into the resonances in Fig. 4b, c, the bulk change causes a shift of the SLR of 6.8 nm and of 5.6 nm for the antisymmetric dimer resonance. This results in simulated bulk sensitivities of 340 nm per RIU for the SLR and 280 nm per RIU for the antisymmetric resonance, which both are a little higher than in the experiment, but still have good agreement. For the thin layer, however, the SLR shifts only by approximately 2.5 nm, whereas the shift of the dimer resonance of 20.1 nm is far stronger, because the near-field only probes the direct vicinity of the particles. This difference reveals that the lattice resonance, which originates from diffraction and is delocalized over the whole array, seems to be better suited for bulk sensing applications, whereas the antisymmetric dimer mode is well suited for molecular sensing.

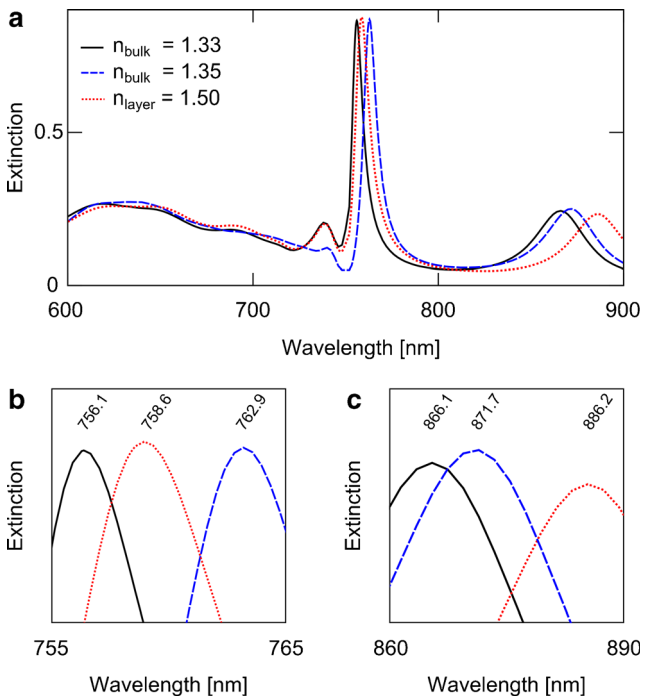

Fig. 4 (**a**) Simulations of the effect of a refractive index change of the bulk immersion liquid from 1.33 to 1.35 (*blue dashed line*) and of a 7 nm thin layer from 1.33 to 1.5 (*red dotted line*) on the SLR and the antisymmetric dimer resonance. (**b**) The zoom into the SLR reveals that it is more sensitive to bulk changes, whereas the antisymmetric mode in (**c**) is very sensitive to changes in a thin layer

Testosterone-antibody sensing

A dimer sensing surface was tested with an immunoassay for the detection of testosterone antibody from a solution. Therefore the nanostructures were coated with a specific recognition structure as shown in Fig. 5a. In the first step the gold dimers were functionalized with short linker molecules. This was done by immersing the substrate in a solution of aminohexanethiol in ethanol with a concentration of 0.84 mg mL^{-1} for 24 h to form a self-assembled monolayer on the gold surface. For the second step testosterone oxime was dissolved (87 mg mL^{-1}) in a solution of diisopropylcarbodiimide in dimethylformamide (concentration of 0.1 mg mL^{-1}). The solution was applied to the sample surface and sandwiched with another glass coverslip. Over 40 h incubation the testosterone oxime was immobilized on the nanostructures' surface by chemical binding to the aminohexanethiol. Finally the sample was rinsed with ethanol and blown dry with nitrogen. A schematic of the process can be seen in Fig. 5a.

The glass coverslip was again mounted onto a PDMS flow cell as described above. A peristaltic pump was connected to the channel with plastic tubing to enable a controlled flow of the solutions.

The sensing experiments were again conducted with the inverted microscope, where the structures were excited by parallel white light from the top through the PDMS, and the extinction of the nanostructure arrays was measured by recording the transmission with the spectrometer. The measurements were performed at a constant flow of the liquids. Spectra were taken in defined steps of time, and the peaks were fitted to obtain the resonance wavelengths. Before the sensing experiments a buffer solution (PBS) was pumped through the flow channel for 1 h. Then solutions of testosterone antibody in PBS, with different concentrations, were run over the surface, each followed by PBS again. For the regeneration of the sensor surface, a sodium dodecyl sulfate solution, which promotes the dissociation of the antibody from the testosterone, was pumped through the channel. To investigate the reproducibility of the process, binding and regeneration was repeated several times in several experiments.

The resonance peak wavelength plotted over time for one concentration series is shown in Fig. 5b for the antisymmetric dimer resonance and in Fig. 5c for the SLR. Antibody binding and regeneration was repeated eight times with different antibody concentrations in the solutions. The total volume of the antibody solution used for each cycle and the flow velocity were kept constant. The flow cell was thus exposed to the antibody solution for the same length of time in each case.

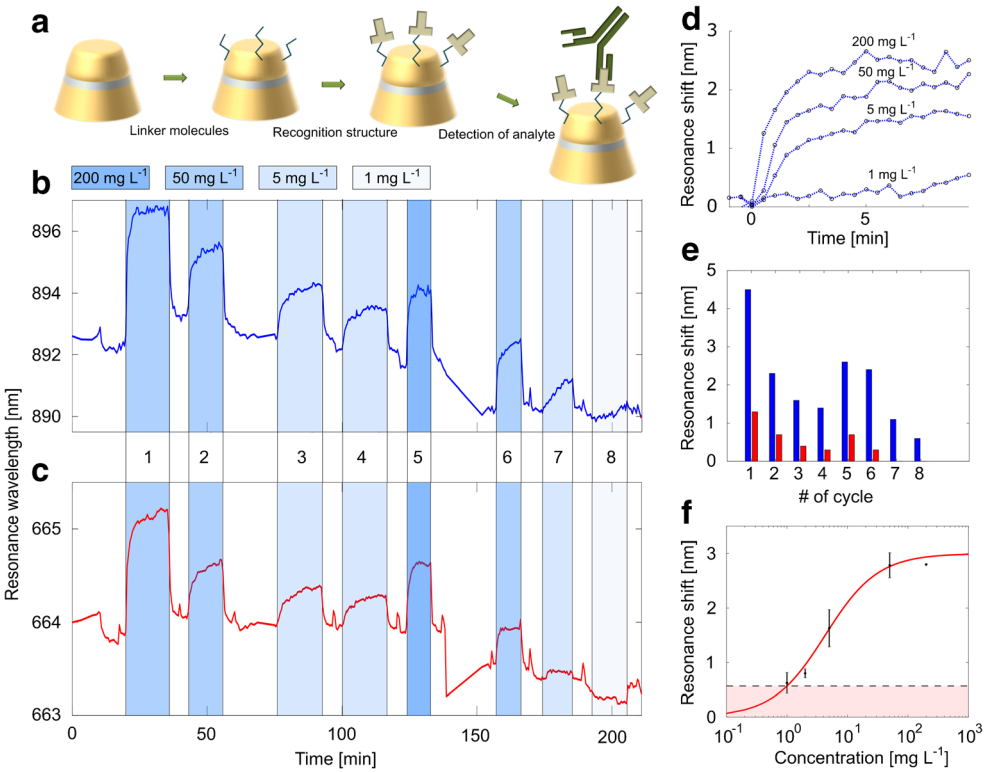

Fig. 5 (**a**) Schematic layout of the sensing surface with specific recognition structure. Peak wavelength of (**b**) the antisymmetric dimer resonance, and (**c**) the surface lattice resonance over time for the different binding and recycling cycles. (**d**) Shift of the antisymmetric resonance over time for different concentrations, followed by PBS buffer after 5 min. (**e**) Maximum peak shift for both resonances for each antibody binding cycle (*left/blue* the antisymmetric dimer resonance, *right/red* the SLR). (**f**) Calibration curve for the sensing surface for the anti-testosterone antibody immunoassay: measured values for 1 mg L^{-1}, 2 mg L^{-1}, 5 mg L^{-1}, 50 mg L^{-1}, and 200 mg L^{-1}. The limit of detection is marked by the *dashed line*

In cycles 1, 2, and 6 a concentration of 50 mg L^{-1} anti-testosterone antibodies was used. Shifts of approximately 4.5 nm, 2.3 nm, and 2.4 nm, respectively, caused by molecule binding were observed for the antisymmetric resonance. The SLR had shifts of 1.3 nm, 0.7 nm, and 0.7 nm, respectively, for this concentration. The stronger shifts of the antisymmetric resonance compared with the SLR are in agreement with the results of the simulations. For cycle 1 the shift was clearly the strongest. This may indicate either that some linker molecules are removed, or that the bound antibodies are incompletely removed in the first regeneration. In cycles 3 and 4 the structures were exposed to 5 mg L^{-1}, with similar results of 1.6 nm and 1.4 nm shifts, respectively, of the antisymmetric resonance (shifts of 0.4 nm and 0.3 nm, respectively, of the SLR). Over cycles 5 to 8 the concentration was decreased from 200 mg L^{-1} through 50 mg L^{-1} and 5 mg L^{-1} to 1 mg L^{-1}. This led to maximum shifts of the antisymmetric mode of 2.6 nm, 2.4 nm, 1.1 nm, and 0.6 nm, respectively. The maximum shifts of the SLR were 0.7 nm and 0.3 nm for cycles 5 and 6, respectively. For the two smallest concentrations no shift of the SLR could be measured.

The time-dependent evolution of the shifts of the antisymmetric resonance for these cycles is shown in Fig. 5d. The number of binding events and thus the resonance shift depends on the kinetics of antibody–antigen binding and the transport from the solution to the structures. The resonance shift was plotted over time, starting when the antibody solution was expected to have reached the flow cell. It increases in a concentration-dependent manner. After 5 min the flow cell was exposed to buffer solution again, and thus no more antibodies were supplied. In this time the concentration-dependent saturation of antibody binding at the structures, and thus the maximum shift for each concentration, was nearly reached for all concentrations. A slight further increase of the shift could be caused by diffusion of antibodies to the buffer solution in the tubes and the flow channel.

Figure 5e shows the maximum resonance shifts (i.e. the shifts of the equilibrium values after binding or, if equilibrium has not been reached, the highest observed values in the plateau) for each of the eight cycles. They were calculated as the differences of the peak wavelengths in buffer solution before and after antibody binding. Compared with the values measured in the early stages of the experiment, a decrease of the shift is observed after some cycles of antibody binding and regeneration for equal antibody concentrations. Also, the resonance wavelength of the structures in the buffer solution shifts slightly to shorter wavelengths over the course of the experiments. This again could be caused by a dissociation of linker molecules in the flow or during the regeneration over time. The effect is stronger for the dimer resonance.

Figure 5f shows a calibration curve for the antisymmetric resonance [28]. The strongest average shifts for high concentrations were approximately 3 nm. A limit of detection was estimated by evaluating the three-sigma limit of the lowest measured concentration of 1 mg L^{-1} [29]. This results in a limit of detection of 0.9 mg L^{-1}, which corresponds to 6 nmol L^{-1} for the investigated antibody.

The selectivity of the antibody sensor was tested by comparing the nonspecific binding of a solution of antibody to mouse IgG and of a BSA solution with the specific binding of anti-testosterone antibody solutions of the same concentrations. In both cases shifts were observed, but these were substantially lower than those observed for the anti-testosterone. Nevertheless, the selectivity still needs to be further optimized.

Conclusions

We investigated arrays of plasmonic vertical dimers for refractive index sensing in a biosensor. The sensitivities of the surface lattice resonance mode and the antisymmetric dimer mode to bulk index changes and to changes in a thin layer were compared. Simulations and experiments revealed that the antisymmetric dimer mode is more sensitive to changes in the direct vicinity of the structures as caused by the binding of molecules. The sensor surface was used in a testosterone immunoassay, and the binding of anti-testosterone antibodies to a specific recognition structure on the nanodimers was repeatably detected for different concentrations.

Acknowledgments This work was financially supported by the Baden-Württemberg Foundation as part of the project GRIN-SEN in the research program Optical Technologies, and by the Deutscher Akademischer Austauschdienst (DAAD) within the scope of the program PROCOPE. The project was performed in the framework of the European Cooperation in Science and Technology COST Action MP1302 Nanospectroscopy. The authors want to thank the partners in the GRIN-SEN and PROCOPE projects for fruitful discussions.

References

1. Haes AJ, Hall WP, Chang L, Klein WL, Van Duyne RP (2004) A localized surface plasmon resonance biosensor: first steps toward an assay for Alzheimer's disease. Nano Lett 4:1029–1034
2. Englebienne P (1998) Use of colloidal gold surface plasmon resonance peak shift to infer affinity constants from the interactions between protein antigens and antibodies specific for single or multiple epitopes. Analyst 123:1599–1603
3. Chen HH, Suzuki H, Sato O, Gu ZZ (2005) Biosensing capability of gold-nanoparticle-immobilized three-dimensionally ordered macroporous film. Appl Phys A Mater Sci Process 81:1127–1130
4. Endo T, Yamamura S, Nagatani N, Morita Y, Takamura Y, Tamiya E (2005) Localized surface plasmon resonance based optical biosensor using surface modified nanoparticle layer for label-free monitoring of antigen–antibody reaction. Sci Technol Adv Mater 6:491–500
5. Eftekhari F, Escobedo C, Ferreira J, Duan X, Girotto EM, Brolo AG, Sinton D (2009) Nanoholes as nanochannels: flow-through plasmonic sensing. Anal Chem 81:4308–4311
6. Mayer KM, Hafner JH (2011) Localized surface plasmon resonance sensors. Chem Rev 111:3828–3857
7. Tittl A, Giessen H, Liu N (2014) Plasmonic gas and chemical sensing. Nanophotonics 3:157–180
8. Lee J, Hasan W, Odom TW (2009) Tuning the thickness and orientation of single Au pyramids for improved refractive index sensitivities. J Phys Chem C 113:2205–2207
9. Fujiwara K, Watarai H, Itoh H, Nakahama E, Ogawa N (2006) Measurement of antibody binding to protein immobilized on gold nanoparticles by localized surface plasmon spectroscopy. Anal Bioanal Chem 386:639–644
10. Kabashin AV, Evans P, Pastkovsky S, Hendren W, Wurtz GA, Atkinson R, Zayats AV (2009) Plasmonic nanorod metamaterials for biosensing. Nat Mater 8:867–871
11. Kim HM, Jin SM, Lee SK, Kim MG, Shin YB (2009) Detection of biomolecular binding through enhancement of localized surface plasmon resonance (LSPR) by gold nanoparticles. Sensors 9:2334–2344
12. Lee SW, Lee KS, Ahn J, Lee JJ, Kim MG, Shin YB (2011) Highly sensitive biosensing using arrays of plasmonic Au nanodisks realized by nanoimprint lithography. ACS Nano 5:897–904
13. Soares L, Csáki A, Jatschka J, Fritzsche W, Flores O, Franco R, Pereira E (2014) Localized surface plasmon resonance (LSPR) biosensing using gold nanotriangles: detection of DNA hybridization events at room temperature. Analyst 139:4964–4973
14. Yakovleva J, Davidsson R, Bengtsson M, Laurell T, Emnéus J (2003) Microfluidic enzyme immunosensors with immobilised protein A and G using chemiluminescence detection. Biosens Bioelectron 19:21–34
15. Pickup JC, Hussain F, Evans ND, Rolinski OJ, Birch DJ (2005) Fluorescence-based glucose sensors. Biosens Bioelectron 20:2555–2565
16. Mayer KM, Hao F, Lee S, Nordlander P, Hafner JH (2010) A single molecule immunoassay by localized surface plasmon resonance. Nanotechnology 21:255503
17. Sherry LJ, Chang SH, Schatz GC, Van Duyne RP, Wiley BJ, Xia Y (2005) Localized surface plasmon resonance spectroscopy of single silver nanocubes. Nano Lett 5:2034–2038
18. Yanik AA, Cetin AE, Huang M, Artar A, Mousavi SH, Khanikaev A, Connor J, Shvets G, Altug H (2011) Seeing protein monolayers with naked eye through plasmonic Fano resonances. Proc Natl Acad Sci U S A 108:11784–11789
19. Auguié B, Barnes WL (2008) Collective resonances in gold nanoparticle arrays. Phys Rev Lett 101:143902
20. Humphrey AD, Barnes WL (2014) Plasmonic surface lattice resonances on arrays of different lattice symmetry. Phys Rev B 90:075404
21. Auguié B, Bendana XM, Barnes WL, de Abajo FJG (2010) Diffractive arrays of gold nanoparticles near an interface: critical role of the substrate. Phys Rev B 82:155447
22. Su KH, Wei QH, Zhang X (2006) Tunable and augmented plasmon resonances of Au SiO_2 Au nanodisks. Appl Phys Lett 88:063118
23. Dmitriev A, Pakizeh T, Käll M, Sutherland DS (2007) Gold–silica–gold nanosandwiches: tunable bimodal plasmonic resonators. Small 3:294–299
24. Ekinci Y, Christ A, Agio M, Martin OJF, Solak HH, Löffler JF (2008) Electric and magnetic resonances in arrays of coupled gold nanoparticle in-tandem pairs. Opt Express 16:13287–13295
25. Pakizeh T, Dmitriev A, Abrishamian MS, Granpayeh N, Käll M (2008) Structural asymmetry and induced optical magnetism in plasmonic nanosandwiches. J Opt Soc Am B 25:659–667
26. Cinel NA, Bütün S, Ertaş G, Özbay E (2013) 'Fairy Chimney'-shaped tandem metamaterials as double resonance SERS substrates. Small 9:531–537
27. Johnson PB, Christy RW (1972) Optical constants of the noble metals. Phys Rev B 6:4370
28. O'Shannessy DJ, Winzor DJ (1996) Interpretation of deviations from pseudo-first-order kinetic behavior in the characterization of ligand binding by biosensor technology. Anal Biochem 236:275–283
29. O'Connell MA, Belanger BA, Haaland PD (1993) Calibration and assay development using the four-parameter logistic model. Chemom Intell Lab Syst 20:97–114